

Epitaxial stabilization and phase instability of VO₂ polymorphs

Shinbuhm Lee, Ilia N. Ivanov, Jong K. Keum & Ho Nyung Lee*

Oak Ridge National Laboratory, Oak Ridge, Tennessee 37831, USA

*hnlee@ornl.gov

The VO₂ polymorphs, i.e., VO₂(A), VO₂(B), VO₂(M1) and VO₂(R), have a wide spectrum of functionalities useful for many potential applications in information and energy technologies. However, synthesis of phase pure materials, especially in thin film forms, has been a challenging task due to the fact that the VO₂ polymorphs are closely related to each other in a thermodynamic framework. Here, we report epitaxial stabilization of the VO₂ polymorphs to synthesize high quality single crystalline thin films and study the phase stability of those metastable materials. We selectively deposit all the phases on various perovskite substrates with different crystallographic orientations. By investigating the phase instability, phonon modes and transport behaviours, not only do we find distinctively contrasting physical properties of the VO₂ polymorphs, but that the polymorphs could be on the verge of phase transitions when heated as low as ~400 °C. Our successful epitaxy of both VO₂(A) and VO₂(B) phases, which are rarely studied due to the lack of phase pure materials, will open the door to the fundamental studies of VO₂ polymorphs for potential applications in advanced electronic and energy devices.

Introduction

Vanadium dioxides (VO_2) are strongly correlated d^1 electron systems and are known to have several polymorphs, which include $\text{VO}_2(\text{A})$, $\text{VO}_2(\text{B})$, $\text{VO}_2(\text{M1})$ and $\text{VO}_2(\text{R})$. While the chemical formula is the same, their crystalline and electronic structures are completely different and highly complex, exhibiting many interesting electrical, optical and chemical properties owing to the strong correlation¹⁻³. Among the aforementioned VO_2 polymorphs, the rutile $\text{VO}_2(\text{R})$ and the monoclinic $\text{VO}_2(\text{M1})$ have been the most widely studied phases due primarily to their metal-to-insulator transition (MIT) temperature close to room temperature (68 °C)¹⁻³. Since this phase transition is accompanied by a huge change in resistivity by three orders of magnitude, $\text{VO}_2(\text{R})$ and $\text{VO}_2(\text{M1})$ have attracted tremendous attention for the electronic and optical applications, such as smart windows⁴, frequency-agile metamaterials^{5,6} and electrical switches⁷⁻⁹.

The monoclinic $\text{VO}_2(\text{B})$ phase has also been explored. However, the focus has been on utilization of the open framework, which originates from the edge-sharing VO_6 octahedra¹⁰⁻¹². Such open framework makes $\text{VO}_2(\text{B})$ a promising energy material, which can be used as electrodes in Li-ion batteries¹³. However, the growth of single crystalline $\text{VO}_2(\text{B})$ has not been very successful due to the complex crystal structure^{14,15}. Similarly, the study of the tetragonal $\text{VO}_2(\text{A})$ has so far been very limited^{16,17} as compared to other VO_2 polymorphs, due to the difficulty in synthesizing phase pure crystals. Thus, their physical properties and potential for technical applications have not been much explored.

One of the main reasons for the difficulty in preparing phase pure VO_2 polymorphs is the narrow range of phase diagram³ and, more importantly, the VO_2

polymorphs are closely related each another in a thermodynamic framework^{10,12,16}. For example, it has been shown that the VO₂(A) and VO₂(B) phases are metastable in bulk and undergo an irreversible phase change into VO₂(R) upon heating^{10,12,16}, resulting in a mixture of VO₂ polymorphs. The formation of such mixed phases hinders the accurate understanding of the physical properties of the VO₂ polymorphs. Hence, preparation of phase pure and high quality crystalline materials has been one of the major challenges in VO₂ research.

Epitaxial stabilization of crystalline materials by formation of low energy interface is a well-known approach to creating pure phase materials^{18–20}. Because the stability of these non-equilibrium materials is affected by both thermodynamic and kinetic factors, the highly non-equilibrium film growth conditions offered by pulsed laser epitaxy (PLE) provides a unique opportunity to discover a wide range of materials with unprecedented functionalities.

Here, we report comparatively the physical properties of four VO₂ polymorphs (i.e., R, M1, A and B phases) epitaxially stabilized by PLE on various perovskite substrates with different crystallographic orientations, i.e., ABO₃(001), ABO₃(011) and ABO₃(111). Distinctively contrasting phase stability, lattice motions and transport properties reported here will provide useful information to develop VO₂-based electronic devices and energy materials.

Results and Discussion

In order to selectively grow VO₂ polymorphs, commercially-available perovskite-oxide substrates, including TbScO₃ (TSO), SrTiO₃ (STO), (LaAlO₃)_{0.3}(Sr₂AlTaO₆)_{0.7}

(LSAT), LaAlO_3 (LAO) and YAlO_3 (YAO), were used. As summarized in Table I, we were able to epitaxially grow (1) the tetragonal $\text{VO}_2(\text{A})$ phase on (011)-oriented STO and LAO substrates; (2) the monoclinic $\text{VO}_2(\text{B})$ phase on a wide selection of (001)-oriented substrates, including pseudo-cubic TSO, STO, LSAT, LAO and pseudo-cubic YAO; and (3) the monoclinic $\text{VO}_2(\text{M1})$ phase on (111)-oriented STO, LSAT and LAO substrates, which commonly have a $3m$ surface symmetry.

The selective growth occurs due to preferential in-plane lattice matching of perovskite-oxide substrates with the VO_2 polymorphs. $\text{VO}_2(\text{B})$ has a low-symmetry monoclinic structure (space group of C2/m) with lattice constants of $a = 12.03 \text{ \AA}$, $b = 3.69 \text{ \AA}$, $c = 6.42 \text{ \AA}$ and $\beta = 106.6^\circ$, as summarized in Table I and as schematically shown in Fig. 1a. Various X-ray diffraction (XRD) scans, including θ - 2θ scans shown in Fig. 2a and ϕ scans (data not shown), for $\text{VO}_2(\text{B})$ films on (001)STO ($a_{\text{STO}} = 3.905 \text{ \AA}$) confirmed the following epitaxy relationship: $(001)\text{VO}_2(\text{B}) \parallel (001)\text{STO}$; $[100]\text{VO}_2(\text{B}) \parallel [100]\text{STO}$. The lattice mismatch $(a_{\text{sub}} - a_{\text{film}})/a_{\text{sub}} \times 100$ was -2.6% for $[010]\text{VO}_2(\text{B}) \parallel [010]\text{STO}$ and $+5.8 \%$ for $[100]\text{VO}_2(\text{B}) \parallel [100]\text{STO}$, where the negative and positive signs indicate compressive and tensile strain, respectively.

$\text{VO}_2(\text{A})$ has a tetragonal structure (space group of $\text{P4}_2/\text{ncm}$) with lattice constants of $a = b = 8.43 \text{ \AA}$ and $c = 7.68 \text{ \AA}$, as schematically shown in Fig. 1b. We found that the single crystalline $\text{VO}_2(\text{A})$ phase could be grown best on (011)STO with the following epitaxy relationship: $(100)\text{VO}_2(\text{A}) \parallel (011)\text{STO}$; $[010]\text{VO}_2(\text{A}) \parallel [011]\text{STO}$, as confirmed by XRD θ - 2θ scans (see Fig. 2b) and ϕ scans (data not shown). The mismatches along the two orthogonal directions, i.e., $[010]\text{VO}_2(\text{A}) \parallel [011]\text{STO}$ and $[001]\text{VO}_2(\text{A}) \parallel [100]\text{STO}$ are -1.7% and $+1.7\%$, respectively.

The VO₂(M1) phase has a low-symmetry monoclinic structure (space group of P2₁/c) with lattice constant of $a = 5.38 \text{ \AA}$, $b = 4.52 \text{ \AA}$, $c = 5.74 \text{ \AA}$ and $\beta = 122.6^\circ$, as schematically shown in Fig. 1c. There have been several reports on the successful growth of VO₂(M1) films on substrates with a $3m$ surface symmetry²¹ such as (0001)Al₂O₃, (111)MgAl₂O₄, (111)MgO and (0001)ZnO. In our study, we mainly attempted to epitaxially grow the films on (111)STO substrates to unify the substrates for VO₂ polymorph films. As shown in Fig. 2c, we found that VO₂(M1) could be grown on (111)STO with the following epitaxy relationship: (010)VO₂(M1) \parallel (111)STO and [010]VO₂(M1) \parallel [111]STO. The lattice mismatch is -3.8% along [001]VO₂(M1) \parallel [1 $\bar{1}$ 0]STO and $+2.6 \%$ along [100]VO₂(M1) \parallel [1 $\bar{1}$ 0]STO.

While the three VO₂ phases listed above are accessible at room temperature from as grown films, we also tried to access to the VO₂(R) phase via a structural phase transition by heating a VO₂(M1) film above the T_c (68 °C). As shown in Fig. 2c, we were able to confirm the phase transition into the VO₂(R) phase by performing an XRD $\theta-2\theta$ scan at 100 °C, which is higher than the T_c . Both VO₂(R) and VO₂(M1) phases on (111)STO are (010)-oriented.

Among the growth parameters, we found that a proper choice of the substrate temperature, T_s , is critical, in particular for VO₂(A) and VO₂(B) phases on perovskite substrates. As shown in Table I, we could reproducibly grow VO₂(A) and VO₂(B) phases when T_s was lower than 430 °C. On the other hand, the growth of VO₂(M1) phase was quite insensitive to T_s as we confirmed the growth of high quality films in a wide temperature window ($400 \leq T_s \leq 600$ °C).

To evaluate the thermal stability of VO₂ polymorphs, epitaxial films of VO₂(A), VO₂(B) and VO₂(M1) phases were heated up to 600 °C. We kept the samples in vacuum (~0.37 Torr) to avoid spontaneous oxidation into V₂O₅ phase²². Figures 3a and b show the phase evolution of VO₂(B)/STO(001) and VO₂(A)/STO(011), respectively, characterized by XRD θ - 2θ scans as a function of temperature. In case of VO₂(B) on STO(001), upon heating, XRD peaks corresponding to 00l VO₂(B) disappeared above 430 °C and then the 330 VO₂(A) peak subsequently appeared above 440 °C, indicating the formation of polycrystalline VO₂(A). When we further increased T_s , the VO₂(A) phase disappeared above 470 °C and the polycrystalline VO₂(R) phase appeared above 520 °C. This transformation, i.e., VO₂(B) \rightarrow VO₂(A) \rightarrow VO₂(R), indicates that the structural frameworks are similar among the phases. The first transition to A-phase is known to associate with the realignment of VO₆ octahedra from edge shared to face shared¹⁰ and, the second transition to the R-phase is attributed to the reorientation of the half of the VO₆ octahedra¹⁰.

As shown in Fig. 3b, the VO₂(A)/STO(011) also revealed similar thermal stability. The peaks corresponding to l00 VO₂(A) disappeared above 430 °C and polycrystalline VO₂(R) was subsequently formed above 470 °C. The phase transitions of both VO₂(B) and VO₂(A) were irreversible upon cooling. The thermal instability of VO₂(A) and VO₂(B) explains the formation of mixed phase VO₂ polymorphs with VO₂(R) as an impurity phase often observed from films grown above 430 °C. The observation of MIT at 68 °C in VO₂(A) and VO₂(B) films grown above 430 °C clearly indicates inclusion of VO₂(R) as an impurity phase¹⁸. We note that, on the other hand, the VO₂(M1) phase was converted into VO₂(R) at ~68 °C upon heating and was stable up to 600 °C (data not

shown). Upon cooling, VO₂(R) was converted back to VO₂(M1), indicating a reversible phase evolution with good thermal stability.

Since the VO₂ polymorphs have distinct structures, one can expect highly contrasting vibrational characteristics of lattice. Thus, identifying the phonon mode is a good measure of phase purity. In order to comparatively understand the phonon modes, Raman spectroscopy was carried out for the VO₂ polymorphs by growing films on LAO substrates. The latter were used because dominant Raman spectral features of LAO are isolated at very low wavelength (32 and 123 cm⁻¹)²³. As shown in Fig. 4, the VO₂ polymorphs revealed contrasting Raman spectra compared to each another. As compared to Raman data available from nanostructured materials^{24–26}, we were able to confirm the phase purity of our epitaxial films.

In addition to the phase confirmation, the Raman spectra from VO₂ provide more detailed information about the local structure. There are three sets of V–O modes²⁷ within wavenumber of 100–1100 cm⁻¹. At low wavenumber (< 400 cm⁻¹), the bands are assigned to V–O–V bending modes; at intermediate wavenumber (400–800 cm⁻¹), the bands are attributed to V–O–V stretching modes; and at high wavenumber (> 800 cm⁻¹), the bands are assigned to V=O stretching modes of distorted octahedral and distorted square-pyramids. As shown in Fig. 4a, the phonon modes in epitaxial films of VO₂(B) were mainly observed at low and intermediate wavenumbers (152, 263 and 480 cm⁻¹), indicating that bending and stretching modes of V–O–V are dominant in VO₂(B). On the other hand, as shown in Fig. 4b, the phonon modes in VO₂(A) were mainly observed at high and intermediate wavenumbers (152, 485 and 887 cm⁻¹), which implies that the stretching modes of V–O–V and V=O are dominant lattice motions in VO₂(A). The

phonon modes in VO₂(M1) are very complex and composed of stretching and bending of V–O–V and zigzag chains of V–V. The phonon modes in VO₂(R) dominantly include stretching modes of V–O–V, which indicates that the crystal structure of VO₂(R) is more symmetric than VO₂(M1)^{26,28,29}.

While the transport properties of VO₂(M1) and VO₂(R) have been extensively studied^{1–3,8,9,22,28–30}, the physical properties of VO₂(B) and VO₂(A) phases have not been much explored due to difficulty in preparing phase pure thin films. Figure 5 shows transport characteristics of VO₂(B), VO₂(A) and VO₂(M1) films grown on STO substrates. VO₂(A) showed a monotonic decrease of resistivity as increasing the temperature, typical for insulators. While still insulating over the temperature range we measured, VO₂(B) revealed more or less semiconducting behaviours with much smaller resistivity compared to that of VO₂(A), i.e., $\rho_{\text{VO}_2(\text{B})}^{300\text{ K}} \approx 0.02\ \Omega \cdot \text{cm}$ and $\rho_{\text{VO}_2(\text{A})}^{300\text{ K}} \approx 60\ \Omega \cdot \text{cm}$. The resistivity in our VO₂(A)/STO(011) is higher than that reported in VO₂(A)/STO(001)²⁰ by one order of magnitude. The reason is unclear, but one can consider that the film on (001)STO is under a different strain state or that the growth on a (001)STO substrate may include a small amount of VO₂(B) since their thermal phase boundary is relatively low^{10,12,16}, as shown in Fig. 3. In the case of VO₂(R) phase, we also observed the MIT at 340 K from VO₂(M1) to VO₂(R) phase change upon heating, similarly observed from many previous studies^{1–3,8,9,22,28–30}. The MIT accompanied a sudden decrease of the resistivity by 3–4 orders of magnitude, which is comparable to high quality epitaxial films grown on Al₂O₃(0001)²². This excellent performance could be attributed to the high crystallinity of our epitaxial films ($\Delta\omega < 0.1^\circ$). The transition temperature is consistent with structural phase transition from VO₂(M1) to VO₂(R), as

shown in XRD θ - 2θ scan in the inset of Fig. 2c. We note that the transport properties of the films grown on LAO substrates were almost identical except for slightly decreased resistivity for films on LAO (data not shown).

Overall, as explained above, the VO₂ polymorphs revealed a wide range of electronic ground states, i.e., metal [VO₂(R)], semiconductor [VO₂(B)] and insulator [VO₂(A) and VO₂(M1)], depending on their crystal structure. This wide range of electronic ground states makes VO₂ highly attractive over other transition metal dioxides, since most other binary oxides have electronic ground states of either metal (CrO₂: α -phase and β -phase) or insulator (TiO₂: rutile, brookite and anatase). While it is not the main focus of this paper, it is worthy mentioning that Goodenough^{28,30} obtained a semiempirical expression for the room temperature critical V-V separation $R_c \approx 2.92$ – 2.94 Å for localized and itinerant 3d electrons in vanadium oxides.

$$R < R_c \rightarrow \text{Itinerant } 3d \text{ electron} \rightarrow \text{Metal};$$

$$R > R_c \rightarrow \text{Localized } 3d \text{ electron} \rightarrow \text{Insulator}.$$

This semiempirical criterion indicates that VO₂ polymorphs can be either metal or insulator depending on V-V separation in the distinguishable crystal structures. The VO₂(R) phase has a uniform V-V separation of $R = 2.87$ Å (refs. 28,29), resulting in a metallic ground state. The VO₂(M1) phase has zigzag V-V chains of $R = 2.60$ Å and 3.19 Å (refs. 28,29). The VO₂(A) phase has zigzag V-V chains of $R = 3.25$ Å, 3.11 Å and 2.78 Å (ref. 17). The insulating behaviours that we have observed for those M1 and A-phases are attributed to the localized electrons in one of V-V chains with $R = 2.60$ Å [VO₂(M1)] and 2.78 Å [VO₂(A)]. Thus, overall transport behaviours of our epitaxial thin films can be well explained by Goodenough's criterion^{28,30}. Since VO₂ polymorphs have

a wide range of physical properties and, in particular, VO₂(B) phase is on the verge of becoming a metal, our report on epitaxial synthesis of high quality thin films can open the door to the discovery of novel phenomena and physical properties by deliberate control of the order parameters by various means, including strain, dimensionality, confinement, etc., which can be accessible via epitaxial heterostructuring.

In conclusion, we grew epitaxial films of VO₂ polymorphs. For the growth of phase pure VO₂ polymorphs, a careful selection of the growth conditions was necessary especially for the temperature and oxygen pressure. Depending on the crystal orientation of substrates, we found that different phases of VO₂ could be selectively grown, i.e., VO₂(B)/ABO₃(001), VO₂(A)/ABO₃(011) and VO₂(M1)/ABO₃(111). Such phases revealed unique phonon modes due to the distinctly different crystal structure and physical properties in spite of the same chemical composition. Since the VO₂ polymorphs have a wide range of electronic ground states from metal [VO₂(R)] and semiconductor [VO₂(B)] to insulator [VO₂(A) and VO₂(M1)], our epitaxial thin films, which are known to be challenging to grow, will expedite our understanding of underlying physics and developing VO₂ polymorphs-based electronic devices utilizing the wide selection of the electronic properties from a single composition.

Methods

Epitaxial film growth. We deposited epitaxial films of VO₂ polymorphs on perovskite oxide substrates by pulsed laser epitaxy. We ablated a sintered VO₂ target by a KrF excimer laser (248 nm in wavelength) at a laser fluence of 1 Jcm⁻² and at a laser

repetition rate of 10 Hz. By growing thin films under a wide range of $P(\text{O}_2)$ and T_s ($10 \text{ mTorr} < P(\text{O}_2) < 25 \text{ mTorr}$ and $350^\circ\text{C} < T_s < 600^\circ\text{C}$), we found the optimal condition for $\text{VO}_2(\text{A})$, $\text{VO}_2(\text{B})$ and $\text{VO}_2(\text{M1})$, as described in Table 1. It should be noted that V_2O_3 is formed at $P(\text{O}_2) < 10 \text{ mTorr}$ and V_2O_5 is formed for $P(\text{O}_2) > 25 \text{ mTorr}$, due to the multivalent nature of vanadium²².

Characterization of physical properties. To investigate the *dc* transport properties, a physical property measurement system (Quantum Design Inc.) was used with Pt contacts in four-probe geometry. X-ray diffraction (XRD) measurements were carried out with a four-circle high-resolution X-ray diffractometer (X'Pert Pro, Panalytical) using the $\text{Cu-K}\alpha_1$ radiation and equipped with a hot stage (DHS 900, Anton Paar). High-temperature environmental XRD measurements were conducted under vacuum with base pressure of 0.37 Torr. Raman spectra were recorded at various temperatures using a temperature control stage (LincamScientific Instruments). A Renishaw 1000 confocal Raman microscope was used to measure Raman spectra in back scattering configuration. Each spectrum is a sum average of seven individual spectra taken at different place on the sample through 20 \times objective. The wavelength of the Raman laser used in these measurements was 532 nm.

Acknowledgements

This work was supported by the U.S. Department of Energy, Office of Science, Basic Energy Sciences, Materials Sciences and Engineering Division. The Raman and high temperature XRD measurements were conducted as a user project at the Centre for

Nanophase Materials Sciences (CNMS), which are sponsored at Oak Ridge National Laboratory by the Scientific User Facilities Division, U.S. Department of Energy.

Author contributions

S.L conceived and designed the experiments under supervision of H.N.L. S.L. fabricated the samples, measured electrical transport and conducted high temperature XRD measurements with help of J.K.K. I.N.I performed Raman spectroscopic measurement. S.L. and H.N.L. wrote the manuscript and other authors reviewed it.

Additional information

Competing financial interests: The authors declare no competing financial interests.

1. Imada, M., Fujimori, A. & Tokura, Y. Metal-insulator transitions. *Rev. Mod. Phys.* **70**, 1039 (1998).
2. Basov, D. N., Averitt, R. D., Van der Marel, D., Dressel, M. & Haule, K. Electrodynamics of correlated electron materials. *Rev. Mod. Phys.* **83**, 471 (2011).
3. Yang, Z., Ko, C. & Ramanathan, S. Oxide electronics utilizing ultrafast metal-insulator transitions. *Annu. Rev. Mater. Res.* **41**, 337 (2011).
4. Zhou, J. *et al.* VO₂ thermochromic smart window for energy savings and generation. *Sci. Rep.* **3**, 3029 (2013).
5. Driscoll, T. *et al.* Mott transition in VO₂ revealed by infrared spectroscopy and nano-imaging. *Science* **325**, 1518 (2009).
6. Liu, M. *et al.* Terahertz-field-induced insulator-to-metal transition in vanadium dioxide metamaterial. *Nature* **487**, 345 (2012).
7. Chang, S. H. *et al.* Oxide double-layer nanocrossbar for ultrahigh-density bipolar resistive memory. *Adv. Mater.* **23**, 4063 (2011).
8. Nakano, M. *et al.* Collective bulk carrier delocalization driven by electrostatic surface charge accumulation. *Nature*, **487**, 459 (2012).
9. Jeong, J. *et al.* Suppression of metal-insulator transition in VO₂ by electric field-induced oxygen vacancy formation. *Science*, **339**, 1402 (2013).
10. Leroux, Ch., Nihoul, G. & Van Tendeloo G. From VO₂(B) to VO₂(R): Theoretical structures of VO₂ polymorphs and *in situ* electron microscopy. *Phys. Rev. B* **57**, 5111 (1998).

11. Chernova, N. A., Roppolo, M., Dillon, A. C. & Whittingham, M. S. Layered vanadium and molybdenum oxides: batteries and electrochromics. *J. Mater. Chem.* **19**, 2526 (2009).
12. Zhang, S. *et al.* From VO₂(B) to VO₂(A) nanobelts: first hydrothermal transformation, spectroscopic study and first principles calculation. *Phys. Chem. Chem. Phys.* **13**, 15873 (2011).
13. Li, W., Dahn, J. R. & Wainwright, D. S. Rechargeable lithium batteries with aqueous electrolytes. *Science* **264**, 1115 (1994).
14. Chen, A. *et al.* Textured metastable VO₂(B) thin films on SrTiO₃ substrates with significantly enhanced conductivity. *Appl. Phys. Lett.* **104**, 071909 (2014).
15. Srivastava, A. *et al.* Selective growth of single phase VO₂(A, B and M) polymorph thin films. *APL Mater.* **3**, 026101 (2015).
16. Oka, Y., Sato, S., Yao, T. & Yamamoto, N. Crystal structures and transition mechanism of VO₂(A). *J. Solid State Chem.* **141**, 594 (1998).
17. Popuri, S. R. *et al.* VO₂(A): Reinvestigation of crystal structure, phase transition and crystal growth mechanisms. *J. Solid State Chem.* **213**, 79 (2014).
18. Schlom, D. G., Chen, L.-Q., Pan, X., Schmech, A. & Zurbuchen, M. A. Strain tuning of ferroelectric thin films. *J. Am. Ceram. Soc.* **91**, 2429 (2008).
19. Choi, W. S. *et al.* Atomic layer engineering of perovskite oxides for chemically sharp heterointerfaces. *Adv. Mater.* **24**, 6423 (2012).
20. Jeon, H. *et al.* Reversible redox reactions in an epitaxially stabilized SrCoO_x oxygen sponge. *Nature Mater.* **12**, 1057 (2013).

21. Wong, F. J., Zhou, Y. & Ramanathan, S. Epitaxial variants of VO₂ thin films on complex oxide single crystal substrates with 3*m* surface symmetry. *J. Cryst. Growth* **364**, 74 (2013).
22. Lee, S., Meyer, T. L., Park, S., Egami, T. & Lee, H. N. Growth control of the oxidation state in vanadium oxide thin films. *Appl. Phys. Lett.* **105**, 223515 (2014).
23. Gasparov, L., Jegorel, T., Loetgering, L., Middey, S. & Chakhalian, J. Thin film substrates from the Raman spectroscopy point of view. *J. Raman Spectrosc.* **45**, 465 (2014).
24. Wu, X., Tao, Y., Dong, L., Wang, Z. & Hu, Z. Preparation of VO₂ nanowires and their electric characterization. *Mater. Res. Bull.* **40**, 315 (2005).
25. Hou, J., Zhang, J., Wang, Z., Zhang, Z. & Ding, Z. Structural transition of VO₂(A) nanorods studied by vibrational spectroscopies. *RSC Adv.* **4**, 18055 (2014).
26. Ji, Y. *et al.* Role of microstructures on the M1-M2 phase transition in epitaxial VO₂ thin films. *Sci. Rep.* **4**, 4854 (2014).
27. Hardcastle, F. D. & Wachs, I. E. Determination of vanadium–oxygen bond distances and bond orders by Raman spectroscopy. *J. Phys. Chem.* **95**, 5031 (1991).
28. Goodenough, J. B. The two components of the crystallographic transition in VO₂. *J. Solid State Chem.* **3**, 490 (1971).
29. Zylbersztejn, A. & Mott, N. F. Metal-insulator transition in vanadium dioxide. *Phys. Rev. B* **11**, 4383 (1975).
30. Goodenough, J. B. Narrow-band electrons in transition-metal oxides. *Czech. J. Phys. B* **17**, 304 (1967).

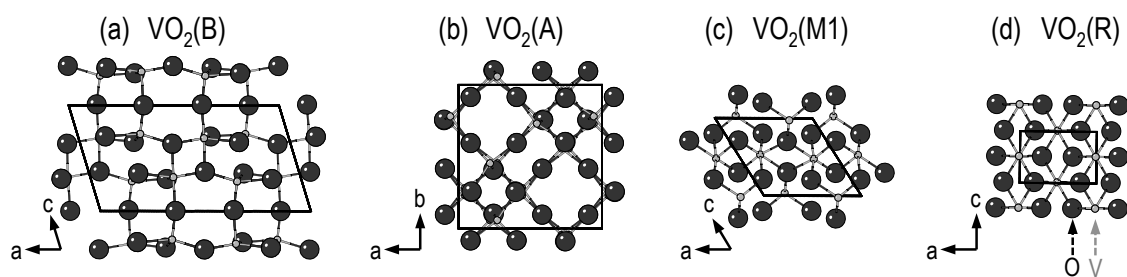


Figure 1 | Schematics of (a) $\text{VO}_2(\text{B})$, (b) $\text{VO}_2(\text{A})$, (c) $\text{VO}_2(\text{M1})$ and (d) $\text{VO}_2(\text{R})$ phases.

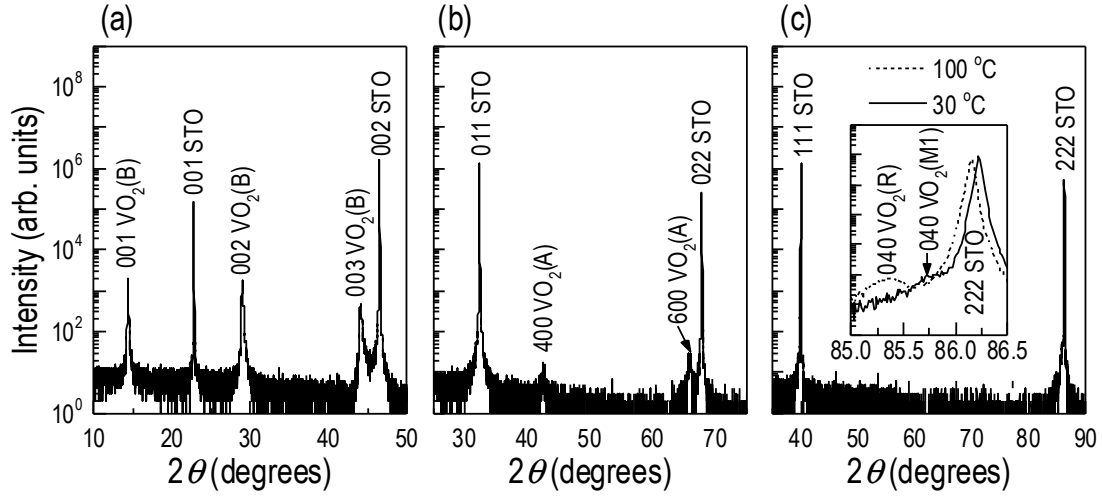


Figure 2 | XRD θ - 2θ scans of (a) VO₂(B), (b) VO₂(A) and (c) VO₂(M1) thin films on STO (001), (011) and (111) substrates, respectively. The inset in (c) shows a XRD scan from the VO₂(R) phase obtained by heating the VO₂(M1) film at 100 °C, which is above the $T_c = 68$ °C.

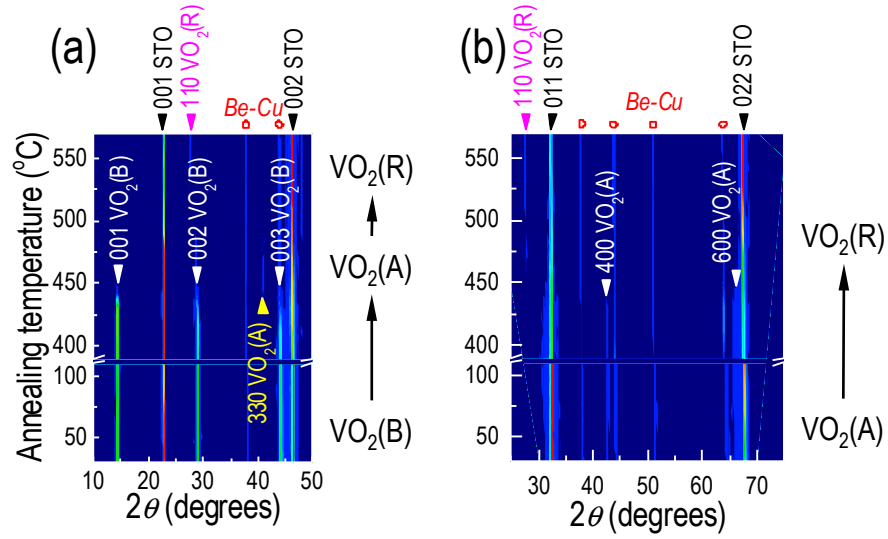


Figure 3 | Real time XRD θ - 2θ scans of (a) $\text{VO}_2(\text{B})/\text{STO}(001)$ and (b) $\text{VO}_2(\text{A})/\text{STO}(011)$ samples as a function of temperature in 0.37 Torr. A clear phase change was observed from both samples, indicating that the phases are in close proximity with each other. The phase changes were, however, irreversible upon cooling.

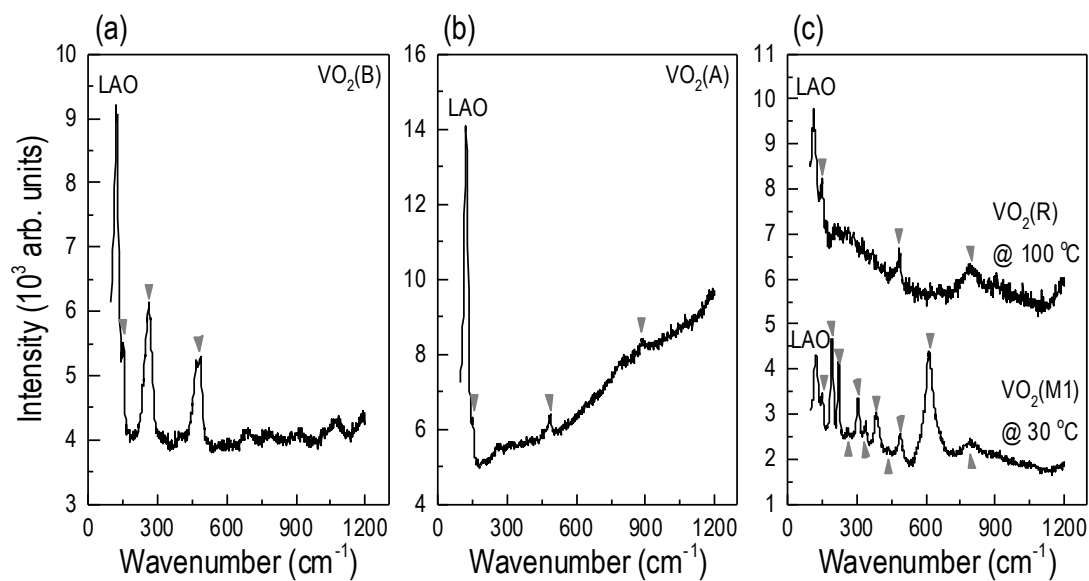


Figure 4 | Raman spectra of (a) VO₂(B), (b) VO₂(A), (c) VO₂(M1) and VO₂(R) grown on LAO substrates. The spectra were recorded at room temperature except the VO₂(R) phase shown in (c), which was obtained by heating the M1 phase sample to 100 °C in air.

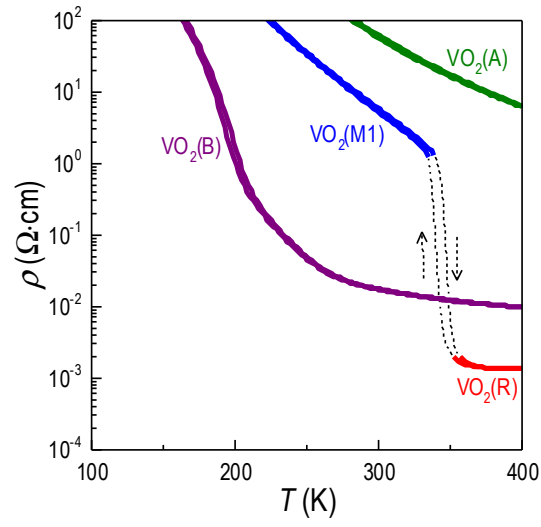


Figure 5 | Temperature dependent resistivity for $\text{VO}_2(\text{B})$, $\text{VO}_2(\text{A})$, $\text{VO}_2(\text{M1})$ and $\text{VO}_2(\text{R})$ phases grown on STO substrates, exhibiting a distinctly contrasting transport behaviour.

Table I | Crystal structure, lattice parameters and growth conditions for VO₂ polymorphs.

VO ₂ polymorphs	Crystal structure (space group)	Lattice constants in bulk				Substrates for epitaxial growth	Critical growth condition
		a (Å)	b (Å)	c (Å)	β (°)		
VO ₂ (A)	Tetragonal (P4 ₂ /ncm)	8.43	8.43	7.68		STO(011), LAO(011)	$T_s < 430$ °C
VO ₂ (B)	Monoclinic (C2/m)	12.03	3.69	6.42	106.6	pc-TSO(001), STO(001), LSAT(001), LAO(001), pc-YAO(001)	$T_s < 430$ °C
VO ₂ (M1)	Monoclinic (P2 ₁ /c)	5.38	4.52	5.74	122.6	STO(111), LSAT(111), LAO(111)	Not critical to T_s
VO ₂ (R)	Tetragonal (P4 ₂ /mmm)	4.55	4.55	2.88		Thermal heating of VO ₂ (M1) above 68 °C	